Available online at website: https://journal.bcrec.id/index.php/bcrec

Bulletin of Chemical Reaction Engineering & Catalysis, 22 (1) 2027, xxx-xxx

Original Research Article

Microwave-Assisted Ni-Zr Impregnation on Bottom-Up Synthesized HZSM-5 for the Transesterification of Sunflower Seed Oil

Muhamad Ilyas Zainul Furqon[1], Vernanda Febrianti[1], Anatta Wahyu Budiman[1,2*], Adrian Nur[1], Bregas Siswahjono Tatag Sembodo[1,2]

[1]Department of Chemical Engineering, Universitas Sebelas Maret, Surakarta, Indonesia.
[2]Interdisciplinary Center of Catalysis and Adsorption, Universitas Sebelas Maret, Surakarta, Indonesia.

Received: 27th August 2026; Revised: 23rd November 2026; Accepted: 24th November 2026
Available online: 30th November 2026; Published regularly: April 2027

Abstract

The transesterification of sunflower seed oil using a heterogeneous HZSM-5 zeolite-based catalyst is one approach to improving biodiesel production efficiency. This study aims to modify HZSM-5 through microwave-assisted Ni-Zr impregnation and to evaluate the effects of the Ni-Zr metal ratio and reaction time on catalytic performance in the transesterification of sunflower seed oil. HZSM-5 was synthesized using the bottom-up method and modified with Ni-Zr via microwave-assisted impregnation at a metal loading of 5% and with varying Ni-Zr ratios of 1:1, 1:2, and 2:1. The catalysts were characterized using XRD, SEM-EDX, BET, and NH_3-TPD. Modification via Ni-Zr impregnation on the HZSM-5 support resulted in changes in crystallinity, crystal size, morphology, particle size, elemental composition, textural properties, and acidity. Catalytic activity was evaluated for the HZSM-5 and Ni-Zr/HZ catalysts at reaction times of 3 and 5 h based on the resulting biodiesel yield. Increasing the reaction time from 3 to 5 h increased the biodiesel yield for all tested catalysts. The best catalytic performance was achieved by the Ni(2)-Zr(1)/HZ catalyst at a reaction time of 5 h, yielding 85.33% biodiesel.

Copyright © 2027 by Authors, Published by BCREC Publishing Group. This is an open access article under the CC BY-SA License (https://creativecommons.org/licenses/by-sa/4.0).

Keywords: Biodiesel; Bottom-up synthesis; Microwave-assisted impregnation; Ni-Zr/ZSM-5 catalyst; Sunflower seed oil

How to Cite: Furqon, M. I. Z., Febrianti, V., Budiman, A. W., Nur, A., Sembodo, B. S. T. (2027). Microwave-Assisted Ni-Zr Impregnation on Bottom-Up Synthesized HZSM-5 for the Transesterification of Sunflower Seed Oil. *Bulletin of Chemical Reaction Engineering & Catalysis*, 22 (1), xxx-xxx. (DOI: 10.9767/bcrec.20829)

Permalink/DOI: https://doi.org/10.9767/bcrec.20829

Supporting Information (SI): https://journal.bcrec.id/index.php/bcrec/article/downloadSuppFile/20829/6606

1. Introduction

Porous materials are widely used in variuos applications because their internal pores and large surface area enable the selective adsorption of reactant molecules, making them suitable for separation and catalytic conversion processes. Porous materials such as amorphous silica, carbon, and clays generally exhibit polydisperse, flexible, and non-discrete pore sizes and structures. In contrast, aluminosilicate zeolites possess homogeneous, rigid, and well-defined pore and channel structures, accompanied by excellent catalytic properties. Zeolites also offer several advantages, including high acidity, thermal stability, chemical resistance, and relatively straightforward synthesis [1].

Zeolites can be synthesized through bottom-up approaches, which involve the direct assembly of zeolite frameworks from molecular or amorphous precursors through hydrothermal processes, in contrast to top-down approaches that modify pre-existing crystalline zeolites. Bottom-up synthesis employs several strategies, including hard-templating, soft-templating, and seed-assisted crystallization. These approaches can produce hierarchical zeolites by introducing intracrystalline mesoporosity into conventional microporous structures or by generating zeolite nanocrystals that from intercrystalline

* Corresponding Author.
Email: budiman@staff.uns.ac.id (A. W. Budiman)

mesopores. Among these methods, conventional hydrothermal synthesis remains one of the most widely employed techniques because it enable effective control over zeolite composition, crystallinity, and pore structure [2].

HZSM-5 is one of the most widely used solid acid catalysts in various catalytic processes. Its catalytic potential is attributed to its distinctive framework structure, tunable porosity, Brønsted and Lewis acid sites, relatively high surface area, and excellent thermal and hydrothermal stability [3,4]. However, biodiesel production still faces several technological challenges, particularly the need for catalysts with high catalytic activity and long-term stability under reaction conditions. Various strategies have been investigated to improve catalyst performance, including modifying the Si/Al ratio [4], incorporating additional elements [5], applying hydrothermal and steam treatments [4], modifying synthesis methods [6], and optimizing operating conditions [7]. Previous studies have indicated that catalyst performance is strongly influenced by several physicochemical properties, including crystallinity [8], specific surface area [9], porous morphology [10], uniform metal dispersion over the support surface [11], and the availability of catalytically active sites [10]. These characteristics are closely related to the type of metal incorporated and the properties of the supporting material.

One promising approach to improving the catalytic properties of HZSM-5 is metal impregnation, particularly through microwave-assisted techniques. Microwave-assisted impregnation offers an alternative modification method that can promote metal dispersion and influence the surface area and crystallinity of the supporting material [12,13]. Previous investigations have demonstrated that bimetallic impregnation, involving combinations such as Cu-Zn, Fe-Mo, and Zn-Ni on HZSM-5, can improve interactions between metal active sites and the acidic sites of zeolites [14-16]. Furthermore, bimetallic catalysts have been reported to exhibit enhanced catalytic activity and improved resistance to deactivation associated with coke formation and metal sintering [17,18].

The incorporation of nickel (Ni) has been reported to improve several physicochemical properties of zeolites, including crystallinity, as indicated by changes in XRD peak intensities and crystal structure ordering [19]. Ni impregnation can also influence particle morphology, resulting in smaller, more spherical particles with relatively uniform distributions and shapes [19-21]. In addition, Ni acts as a catalytic promoter by modifying the strength and distribution of acid sites, influencing crystallinity, and optimizing surface morphology, thereby potentially enhancing catalytic activity and suppressing coke formation [19,21]. Pandiangan *et al.* [22] reported that Ni incorporation into ZSM-5 improved catalytic activity compared with that of unmodified ZSM-5, achieving an oil conversion of up to 100% and a methyl ester yield exceeding 90%. The resulting methyl ester composition consisted of methyl stearate (54.02%), methyl palmitate (25.45%), and methyl oleate (14.89%).

In addition to Ni, zirconium (Zr) has also attracted attention as a metal modifier for ZSM-5 catalysts. Yusuf *et al.* [23] reported that incorporating Zr into ZSM-5 resulted in an oil conversion of 97.84%, which was attributed to improvements in active site availability, mesoporous structure, specific surface area, and overall acidity. Moreover, the Zr/ZSM-5 catalyst maintained an oil conversion of 93.8% after three consecutive reuse cycles, indicating its potential for catalytic reuse. Similarly, Su *et al.* [24] demonstrated that Zr/ZSM-5 could enhance catalytic activity through increased acidity, achieving a polyol ester yield of 94.41%. These findings indicate that both Ni and Zr can individually contribute to improving the catalytic properties of ZSM-5, although their effects may differ depending on the metal incorporated and the resulting physicochemical characteristics.

Biodiesel is a type of bioenergy consisting of alkyl esters, particularly fatty acid methyl esters (FAME), derived from long-chain fatty acids (C_{14}–C_{24}) obtained from plant or animal lipids, such as vegetable oils, animal fats, and used cooking oil [25]. According to Eldwita *et al.* [26], commonly used vegetable oil feedstocks for biodiesel production include soybean oil, palm oil, castor oil, corn oil, kemiri sunan oil, rubber seed oil, nyamplung seed oil, kepayang seed oil, kapok seed oil, and sunflower seed oil. In this study, sunflower seed oil was selected as the feedstock for biodiesel production. Sunflower seed oil primarily contains unsaturated fatty acids, particularly linoleic acid (44–72%) and oleic acid (14–43%), along with saturated fatty acids such as palmitic acid (4–9%) and stearic acid (1–7%). Furthermore, sunflower seeds have a relatively high oil content, ranging from 48 to 52% [27]. These characteristics make sunflower seed oil a promising feedstock for biodiesel production as an alternative to fossil-based fuels.

Transesterification is one of the most widely employed methods for biodiesel production because of its high conversion efficiency, relatively mild operating conditions, and lower production costs compared with other processes. In this reaction, triglycerides react with alcohol to form diglycerides and subsequently monoglycerides, ultimately producing glycerol and FAME. Several factors influence transesterification performance, including the alcohol-to-oil molar ratio, catalyst type and concentration, reaction temperature,

Copyright © 2027, ISSN 1978-2993

reaction time, moisture content, and free fatty acid (FFA) concentration [28].

Although previous studies have demonstrated the catalytic benefits of Ni and Zr incorporation into ZSM-5, most investigations have focused on the individual effects of these metals or other bimetallic combinations. For instance, Ni-modified ZSM-5 has been investigated for improving catalytic activity and methyl ester production, whereas Zr-modified ZSM-5 has been reported to enhance acidity, porosity, and catalytic stability. However, the combined incorporation of Ni and Zr into HZSM-5 for the transesterification of sunflower seed oil has not yet been systematically investigated. In particular, the influence of different Ni-Zr loading ratios on the structural, textural, and acidic properties of HZSM-5, as well as the relationship between these properties and catalytic performance, remains insufficiently understood.

Therefore, the novelty of this study lies in the integration of microwave-assisted bimetallic Ni-Zr impregnation with bottom-up synthesized HZSM-5 and its application as a heterogeneous catalyst for sunflower seed oil transesterification. Unlike previous studies investigating Ni or Zr separately, this research systematically evaluates different Ni-Zr loading ratios to elucidate their effects on catalyst crystallinity, crystal characteristics, morphology, elemental composition, textural properties, and acidity. Furthermore, the relationship between these physicochemical properties and catalytic performance is investigated to determine how bimetallic composition influences biodiesel production. This approach provides new insights into the structure-property-performance relationship of Ni-Zr-modified HZSM-5 catalysts and their application in biodiesel production.

Based on the aforementioned research gap, this study aims to synthesize HZSM-5 through a bottom-up hydrothermal approach and subsequently modify it through microwave-assisted bimetallic Ni-Zr impregnation at different metal loading ratios. The modification is intended to tailor the physicochemical properties of HZSM-5, particularly its crystallinity, morphology, porosity, and acidity, to improve its catalytic performance in sunflower seed oil transesterification. The resulting catalysts are characterized using XRD, SEM-EDX, BET, and NH_3-TPD analyses to investigate their elemental composition, structural properties, morphology, textural characteristics, and acidity. Furthermore, their catalytic performance is evaluated based on biodiesel yield at different reaction times. Through this investigation, the study seeks to establish the relationship between Ni-Zr composition, catalyst physicochemical properties, and catalytic performance, thereby identifying the Ni-Zr loading composition and reaction conditions that provide the best performance for biodiesel production.

2. Materials and Methods

2.1. Materials

The materials used in this research was Sunflower seed oil from local market in Semarang. The chemical used for this study included aluminium isopropoxide ($Al(OCH(CH_3)_2)_3$, Loba Chemie, Cat.No.0091200500), ludox (SiO_2 30 %wt, Aldrich, Cat.No.420794-1L), sodium hydroxide (NaOH 99 %wt, Merck, Cat.No.1.06498.1000), tetrapropylammonium bromide (TPABr 99 %wt, Merck, 225568-100G), ammonium nitrate (NH_4NO_3, Merck, Cat.No.1011881000), distilled water (H_2O), methanol (CH_3OH, Merck, Cat.No.1.06009.1000), transition metal precursors: nickel(II) nitrate hexahydrate ($Ni(NO_3)_2.6H_2O$, Merck, Cat.No.1.06721.0250), and zirconium (IV) oxynitrate hydrate ($ZrO(NO_3)_2.H_2O$, Aldrich, Cat.No.243493-100G). A stainless-steel hydrothermal reactor (HTR) with a Teflon cup of 100 mL was used for zeolite HZSM-5 bottom-up synthesis.

2.2. Synthesis Zeolite HZSM-5

HZSM-5 was synthesized via a hydrothermal method using a molar rasio of $10Na_2O : 50SiO_2 : 1Al_2O_3 : 20TPABr : 1800H_2O$. NaOH and colloidal silica were mixed, while TPABr and aluminium isopropoxide were separately dissolved in H_2O. The NaOH-silica and TPABr solutions were mixed under continuous stirring, followed by the addition of the aluminium isopropoxide solution. The mixture was vigorously stirred at 2000 rpm for 5 h until a homogeneous gel was obtained. The gel was subsequently aged for 72 h at room temperature and then subjected to hydrothermal crystallization in an autoclave at 180 ^oC for 48 h. The resulting solid was washed with distilled water, dried at 110 ^oC overnight, and calcined at 550 ^oC for 3 h to remove the organic template, yielding Na-ZSM-5. Ion exchange was then performed using 1 mol/L NH_4NO_3 solution at 80 ^oC for 2 h with a solution to solid rasio of 10 mL/g, and process was repeated twice. The resulting NH_4-ZSM-5 was dried at 110 ^oC overnight and calcined at 550 ^oC for 6 h to decompose the NH_4^+ ions and obtain HZSM-5. The bottom-up synthesis is illustrated in Figure 1.

2.3. Impregnation Ni-Zr into Support HZSM-5

Ni-Zr/HZSM-5 catalysts were synthesized using microwave-assisted impregnation method. Ni-Zr was impregnated on HZSM-5 by incipient wetness impregnation with 5% loading and variations ratio 1:1, 1:2, and 2:1 of metals in catalyst. First, the solution of $Ni(NO_3)_2.6H_2O$ and

Copyright © 2027, ISSN 1978-2993

$ZrO(NO_3)_2.H_2O$ were put into support HZSM-5, and each was impregnated for 2 h. Then, microwave-assisted heating was performed at 500 watt for 15 minutes. Then, the samples were dried in oven at 110 °C to remove the water. After that, the samples were calcined at 500 °C for 4 h. The obtained catalysts were named Ni(1)-Zr(1)/HZ, Ni(1)-Zr(2)/HZ, and Ni(2)-Zr(1)/HZ. The impregnation Ni-Zr into support HZSM-5 with microwave-assisted illustrated in Figure 2.

2.4. Catalyst Characterizations

The prepared HZSM-5 commercial, synthesis, Ni(1)-Zr(1)/HZ, Ni(1)-Zr(2)/HZ, and Ni(2)-Zr(1)/HZ catalyst were analyzed by using several instruments, including X-Ray Diffraction (XRD) with diffractometer (Rigaku MiniFlex) was used to determine the crystalline structure of the catalysts using the Cu-Kα radiation operated at voltage 40 kV, and 30 mA. Scanning Electron Microscopy-Energy Dispersive X-ray (SEM Jeol JSM-IT200) was used to determine the morphology of catalysts as well as metal contents. The textural properties of the catalyst, i.e., surface area, pore volume, and average pore diameter, were characterized by Nitrogen physisorption (Quantachrome Quadrasorb EVO). The acidic properties of the catalysts were characterized using NH_3-TPD (Chemisorb 2750).

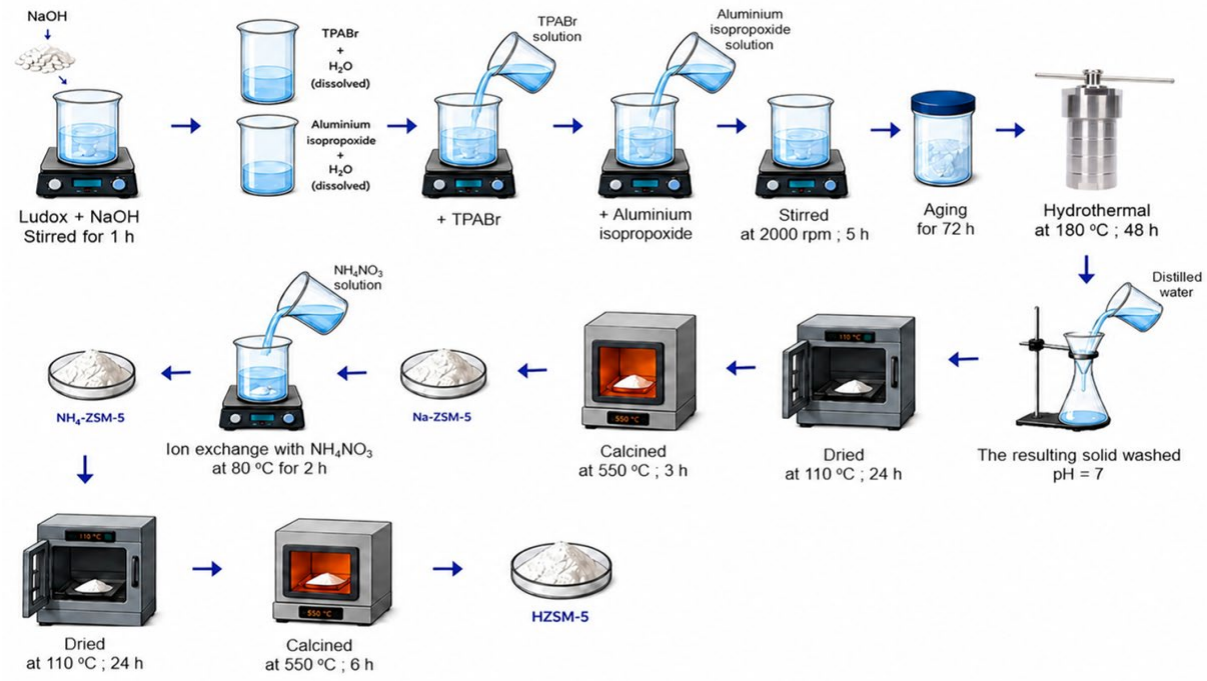


Figure 1. Bottom-up method synthesis route of HZSM-5.

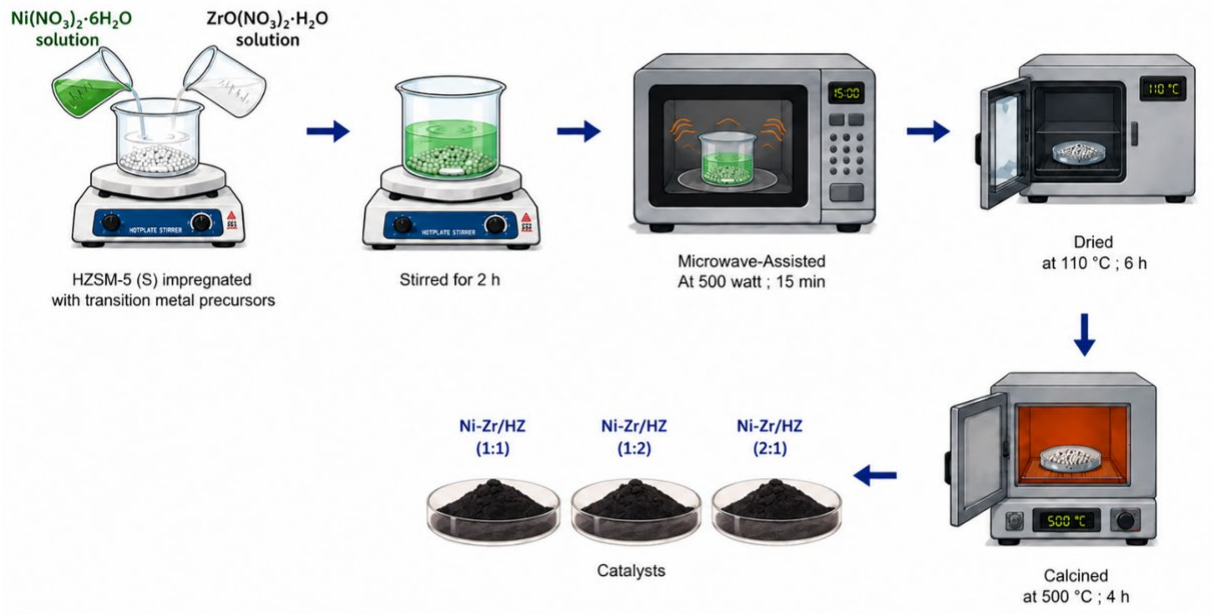


Figure 2. Impregnation Ni-Zr with microwave-assisted into support HZSM-5.

Copyright © 2027, ISSN 1978-2993

2.5. Transesterification of Sunflower Seed Oil

The prepared catalysts HZSM-5 (C), HZSM-5 (S), Ni-Zr/HZ loading 5% (1:1, 1:2, and 2:1). First, 40 gram of sunflower seed oil is put into a 250 mL beaker, then added with 27.74 mL of methanol (oil: methanol ratio (1:15)), then added with 3 %wt of catalyst that has been prepared. Next stirred at 60 °C for 3 and 5 h. The samples that have been made are filtered to separate the product from the catalyst. Next, the product was left overnight in a separatory funnel to separate the FAME from the gliserol. After that the sample is put in a bottle, labeled, and allowed to stand for one night. The Experimental setup for the transesterification illustrated in Figure 3.

2.6. Design of Experiments (DOE)

The experimental design in this research was conducted using multilevel factorial design (5×2), catalyst type and transesterification reaction time. The catalyst factor consisted of five levels, namely HZSM-5 (C), HZSM-5 (S), Ni(1)-Zr(1)/HZ, Ni(1)-Zr(2)/HZ, and Ni(2)-Zr(1)/HZ, while the reaction time factor consisted of two levels, namely 3 and 5 h. Thus, a total of 10 treatment combinations were obtained. The experimental design is presented in Tabel 1. After conducting the experiments according to all predetermined variations, the experimental data were analyzed using Minitab to determine the significance of each factor and their interaction on biodiesel yield. Analysis of variance (ANOVA) was performed to evaluate the statistical significance of the catalyst type and reaction time. The analysis was performed at a 5% significance level (α = 0.05), with the null hypothesis (H_0) stating that there is no difference in mean yield among treatments, while the alternative hypothesis (H_1) states that there is a difference in mean yield. Decisions were made based on the p-value, H_0 was rejected if the p-value was < 0.05, indicating a significant effect of catalyst type and reaction time on biodiesel yield. The mathematical model representing biodiesel yield is given by equation (1):

$$Y = \beta_0 + \beta_1 X_1 + \beta_2 X_2 + \beta_3 X_3 + \beta_4 X_4 + \beta_5 X_5 + \beta_6 X_6 + \beta_7 X_7 \quad (1)$$

whereas, X_1 is HZSM-5 (C), X_2 is HZSM-5 (S), X_3 is Ni(1)-Zr(1)/HZ, X_4 is Ni(1)-Zr(2)/HZ, X_5 is Ni(2)-Zr(1)/HZ, X_6 is 3 hours, X_7 is 5 hours, and β is the coefficient of regression on each factor. Tabel 1 shows the experimental design of this study.

3. Results and Discussion

3.1 Synthesis Zeolite HZSM-5

HZSM-5 zeolite was produced hydrothermally with an initial molar composition

Table 1. Experimental design.

Catalyst	Reaction Time (h)	Yield (%)
HZSM-5 (C)	3	65.32
HZSM-5 (C)	5	70.57
HZSM-5 (S)	3	71.07
HZSM-5 (S)	5	72.70
Ni(1)-Zr(1)/HZ	3	76.72
Ni(1)-Zr(1)/HZ	5	79.17
Ni(1)-Zr(2)/HZ	3	76.66
Ni(1)-Zr(2)/HZ	5	78.33
Ni(2)-Zr(1)/HZ	3	84.27
Ni(2)-Zr(1)/HZ	5	85.33

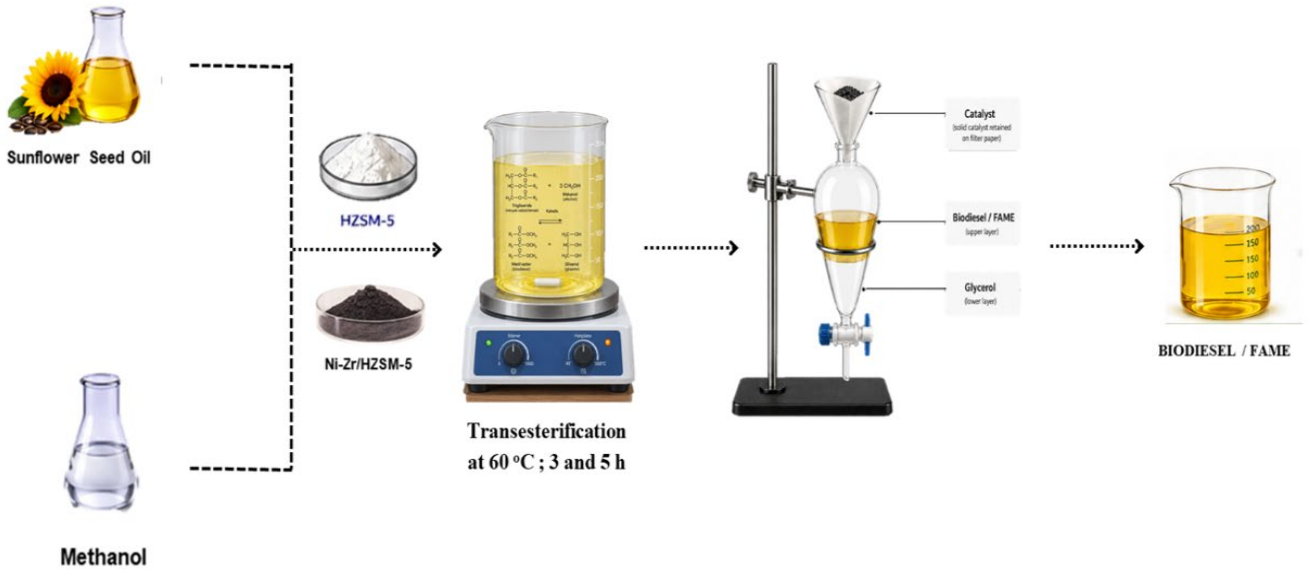


Figure 3. Experimental setup for the transesterification of sunflower seed oil using catalyst HZSM-5 and Ni-Zr/HZSM-5.

Copyright © 2027, ISSN 1978-2993

of $10Na_2O : 50SiO_2 : 1Al_2O_3 : 20TPABr : 1800H_2O$. To begin the synthesis, precursor solutions were prepared. These included sodium hydroxide (NaOH) as a source of Na_2O, aluminum isopropoxide as a source of Al_2O_3, tetrapropylammonium bromide (TPABr) as a structure-directing agent (SDA), Ludox as a source of SiO_2, and distilled water as a solvent. The result is still in the form of Na-ZSM-5; thereafter, ion exchange is performed using an NH_4NO_3 solution to replace the Na^+ ions in the zeolite framework with NH_4^+ ions [29]. After ion exchange, the white solid is washed, dried, and calcined at 550 °C for 6 hours to decompose NH_4^+ ions into NH_3, leaving H^+ ions at the zeolite framework sites and yielding HZSM-5 with Brønsted acid sites. The presence of these acid sites is critical for active catalytic centers [30] and serves as the foundation for subsequent modification by microwave-assisted Ni-Zr metal impregnation. The HZSM-5 zeolite product had an average final weight of 4.8065 grams, with a yield of 80.51%.

3.2. Catalyst Characterizations

The XRD study results in Figure 4 reveal that the diffraction pattern of the synthesized HZSM-5 sample is identical to that of commercial HZSM-5, with a typical MFI crystal structure and an orthorhombic crystal system. Peaks appear in the range of 7.93-45.01°, notably at 2θ = 7.93°; 8.85°; 14.76°; 15.90°; 20.81°; 23.05°; 23.27°; 23.67°; 23.91°; 24.36°; 29.27°; 29.87°; 44.69° and 45.01°. This pattern corresponds to the standard in ICDD No. 00-044-0003, which indicates that the HZSM-5 peaks appear at 2θ = 7.97°; 8.82°; 14.79°; 15.92°; 20.87°; 23.08°; 23.32°; 23.72°; 23.95°; 24.41°; 29.28°; 29.86°; 45.05°; 45.53°.

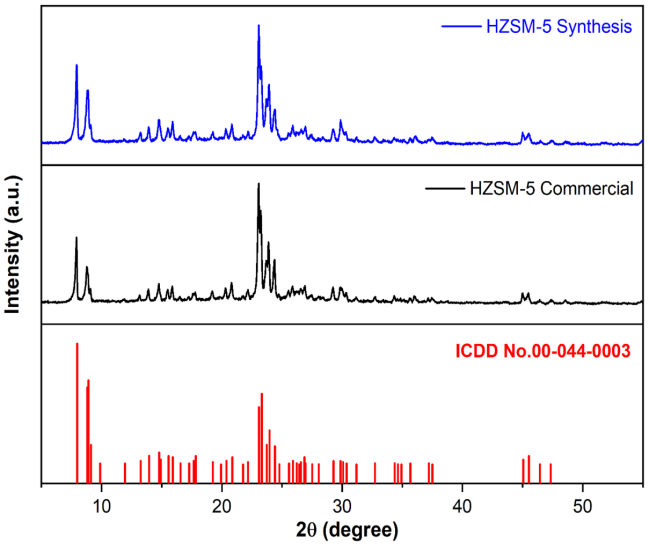


Figure 4. XRD diffractograms of HZSM-5 commercial and synthesis.

The calculation results show that the relative crystallinity of commercial HZSM-5 zeolite and the synthesized sample were 90.33% and 93.11%, respectively, and the average crystal sizes computed using the Scherrer equation were 52.08 and 45.56 nm, as given in Table 1 ???. These crystallinity values show that the synthesized HZSM-5 zeolite has a well-formed MFI crystal structure that is somewhat greater than commercial HZSM-5. The creation of high crystallinity is directly linked to the processes of crystal nucleation and growth during the hydrothermal process.

Initially, the silicate and aluminate species are polymerized to form crystal nuclei. The structure-directing agent (SDA) TPABr then controls the arrangement of the zeolite building blocks, resulting in an ordered MFI framework. According to Anekwe *et al.* [31], this consistency is demonstrated by the presence of sharp, characteristic HZSM-5 diffraction peaks in the XRD pattern with relatively high intensity, indicating that the synthesis process successfully produced the HZSM-5 crystalline phase without the formation of significant impurity phases. Furthermore, the crystal size of the produced material remained within the range described in the study by Duan *et al.* [32], which is roughly 40 nm. These findings are also compatible with Castillo *et al.*'s interpretation [33], which said that sharp and narrow peaks in the diffractogram indicate high crystallinity and big crystal size, whereas widened peaks suggest low crystallinity (amorphous) and small crystal size.

The XRD analysis results in Figure 5 show that the diffraction patterns for the Ni(1)-Zr(1)/HZ, Ni(1)-Zr(2)/HZ, and Ni(2)-Zr(1)/HZ catalysts, resulting from the addition of Ni and Zr metals to the HZSM-5 support show Ni metal peaks at 2θ = 36.74° (c) and 43.22° (c), which are consistent with the standard pattern for cubic-phase nickel oxide (NiO) in ICDD No. 01-078-0643. Furthermore, zirconium (Zr) peaks emerged at 2θ = 26.36° (m), 31.35° (t), and 36.25° (t), corresponding to the tetragonal phase of zirconium oxide (ZrO_2) as specified in ICDD No. 00-050-1089 and the monoclinic phase as defined in ICDD No. 00-037-1484. These findings show

Table 2. Crystallinity and crystal size of the catalyst.

Catalyst	Crystal Size (nm)	Crystallinity (%)
HZSM-5 (C)	52.08	90.33
HZSM-5 (S)	45.56	93.11
Ni(1)-Zr(1)/HZ	37.94	96.19
Ni(1)-Zr(2)/HZ	35.08	92.65
Ni(2)-Zr(1)/HZ	38.86	97.05

Copyright © 2027, ISSN 1978-2993

that Ni and Zr metals were successfully incorporated into the surface and pores of the HZSM-5 support. Based on the XRD patterns after impregnation, these results are consistent with the findings of Anekwe *et al.* [31], reported that the XRD patterns were successfully retained despite the addition of metals; however, in their study, the diffraction patterns of metal oxides were very weak and nearly undetectable.

Crystallinity increased with metal addition, as indicated in Table 2 for the Ni(1)-Zr(1)/HZ and Ni(2)-Zr(1)/HZ catalysts, reaching 96.19% and 97.05%, respectively, with the maximum crystallinity recorded after adding more Ni (2:1). This is similar with the findings of Anekwe et al. [31], discovered that the XRD diffraction pattern intensity of Ni/HZSM-5 was greater than that of pure HZSM-5 or Co/HZSM-5, showing that crystallinity increases after Ni impregnation. Meanwhile, in this investigation, the Ni(1)-Zr(2)/HZ catalyst, which used a higher amount of Zr (1:2), showed a drop in crystallinity of 92.65%. Brioual *et al.* [34] suggest that Zr^{4+} ions have a large ionic radius, which causes mechanical distortion in the HZSM-5 support crystal lattice. According to Eviva *et al.* [35], the intensity difference occurs because the number of crystal planes generated in each sample differs, resulting in varying amounts of light reflected from the crystal planes. Samples that reflect more light yield more intensity, indicating that the final zeolite product has a higher crystallinity.

Furthermore, as shown in Table 2, the crystal size reduced with metal addition, from 45.56 nm for the Ni(1)-Zr(1)/HZ, Ni(1)-Zr(2)/HZ, and Ni(2)-Zr(1)/HZ catalysts to 37.94, 35.08, and 38.86 nm, respectively. These findings are consistent with those reported by Hu *et al.* [36], Chaisamphao *et al.* [37], and Liu *et al.* [38], found that Ni impregnation can reduce particle size and create active interface sites, enhancing catalytic performance. Table 2 displays crystallinity and crystal size for the HZSM-5 (C), HZSM-5 (S), and Ni(1)-Zr(1)/HZ, Ni(1)-Zr(2)/HZ, and Ni(2)-Zr(1)/HZ catalysts.

The SEM study results displayed in Figure 6 were acquired at a magnification of 5,000×. It is clear that HZSM-5 impregnated with Ni-Zr metal has a blocky-prismatic shape at all metal ratios. The morphology of the Ni(1)-Zr(1)/HZ catalyst reveals that a portion of the crystal surface is becoming covered by tiny particles caused by metal deposition. Metal dispersion is reasonably homogeneous, and tiny metal agglomerates were found. Furthermore, HZSM-5 impregnated with Ni-Zr (1:2) has rather consistent metal dispersion. However, the quantity of metal particles on the crystal surface has risen, and some have agglomerated. This is owing to a larger Zr concentration, which causes more metal deposition. Finally, the Ni(2)-Zr(1)/HZ catalyst

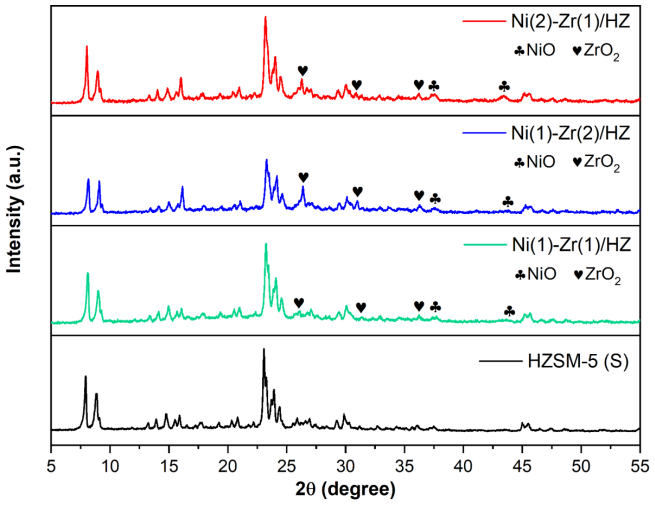


Figure 5. XRD diffractograms of HZSM-5 (S), Ni(1)-Zr(1)/HZ, Ni(1)-Zr(2)/HZ, dan Ni(2)-Zr(1)/HZ.

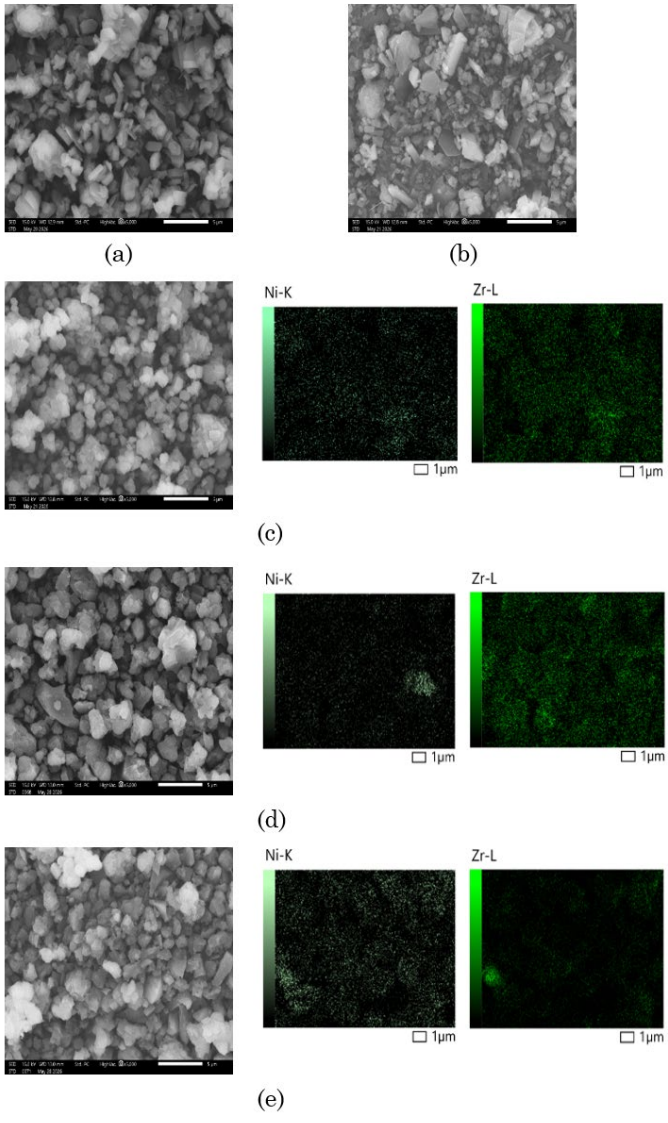


Figure 6. SEM Images of (a) HZSM-5 (C), (b) HZSM-5 (S), (c) Ni(1)-Zr(1)/HZ, (d) Ni(1)-Zr(2)/HZ, and (e) Ni(2)-Zr(1)/HZ.

Copyright © 2027, ISSN 1978-2993

has reasonably homogeneous metal dispersion. However, the surface seems denser as a result of the metal particles that have adhered. The distribution of metal particles appears more homogenous, and the agglomeration size is smaller than in the 1:2 ratio. This suggests that increasing Ni leads to improved metal dispersion. The impregnation mechanism in our work is consistent with that reported by Adany *et al.* [39], found that following impregnation, metal particles agglomerate and distribute uniformly within the support. These findings are supported by a study conducted by Niu *et al.* [40], which explains that, when compared to single metal oxides, the addition of bimetallic elements is more likely to affect catalyst structure; this is due to the ease with which agglomeration occurs during the calcination process, which is caused by the high content of bimetallic oxides.

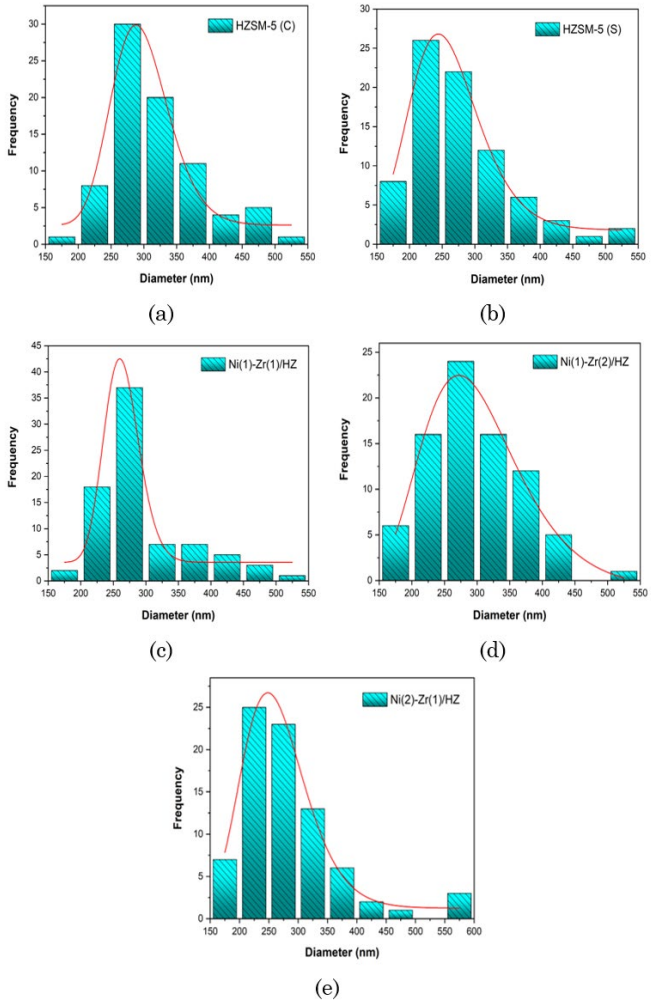


Figure 7. Particle size distribution of (a) HZSM-5 (C), (b) HZSM-5 (S), (c) Ni(1)-Zr(1)/HZ, (d) Ni(1)-Zr(2)/HZ, and (e) Ni(2)-Zr(1)/HZ.

According to the particle size distribution graphs in Figure 7 and Table 3, the average particle sizes for commercial and synthesized HZSM-5 were 317.33 and 277.83 nm, respectively. These results are lower than those published by Duan *et al.* [32], said that commercial HZSM-5 typically has particle sizes in the micron range, precisely 1.5 m. These lower particle sizes have a reasonably homogeneous distribution, indicating that the synthesis process resulted in particles that were highly uniform. Following the Ni-Zr metal impregnation procedure, the particle size distribution graph indicated average particle sizes for Ni(1)-Zr(1)/HZ, Ni(1)-Zr(2)/HZ, and Ni(2)-Zr(1)/HZ of 293.97, 296, and 283.85 nm, respectively. Table 4.6 ??? shows that particle sizes increased during the Ni-Zr metal impregnation procedure. Zhang *et al.* [41] found that increasing Ni metal loading on CeO_2 decreases electrical interactions with the support, resulting in larger Ni particle sizes.

Figure 8 shows the isotherm curves for all samples, which are Type IV. These results are typical of mesoporous materials classified by the IUPAC, with a wide hysteresis loop ranging from $0.45 < P/P_0 < 0.9$. These findings are consistent with the findings of Anekwe *et al.* [31], found that HZSM-5, both as synthesized and after Ni-Zr modification, exhibits a type IV adsorption-desorption isotherm with a hysteresis loop ranging from $0.45 < P/P_0 < 1.0$, with a larger hysteresis loop indicating that the sample contains a substantial mesoporous framework.

Table 3. Catalyst particle size.

Catalyst	Particle Size (nm)
HZSM-5 (C)	317.33
HZSM-5 (S)	277.83
Ni(1)-Zr(1)/HZ	293.97
Ni(1)-Zr(2)/HZ	296.00
Ni(2)-Zr(1)/HZ	283.85

Table 4. Properties of HZSM-5 and Ni-Zr/HZ catalyst.

Catalyst	Surface Area (m^2/g)	Pore Size (nm)	Pore Volume (cm^3/g)	Element (wt%)	
				Ni	Zr
HZSM-5 (C)	345.930	2.559	0.2213	-	-
HZSM-5 (S)	315.255	2.838	0.2237	-	-
Ni(1)-Zr(1)/HZ	327.615	3.273	0.2680	3.34	0.68
Ni(1)-Zr(2)/HZ	269.266	3.817	0.2570	4.09	5.00
Ni(2)-Zr(1)/HZ	246.558	3.007	0.1854	7.33	3.80

Copyright © 2027, ISSN 1978-2993

Table 4 shows that the commercial and synthesized HZSM-5 zeolites have surface areas of 345.93 and 315.255 m²/g, respectively. Anekwe *et al.* [31] reported a surface area of 397.5 m²/g for synthesized HZSM-5 with a Si/Al ratio of 40, but their values are lower. This discrepancy is most likely due to the greater Si/Al ratio in this sample, which was 50. At a Si/Al ratio of 40, the internal pore structure and framework geometry improve N_2 gas accessibility during surface area characterisation with the BET method. Several investigations have reported that the surface area of synthesized HZSM-5 is virtually equal to that observed in this study namely, 342.957 m²/g [42] and 321.158 m²/g [43], with Si/Al ratios larger than 50.

According to Table 4, the surface area of the Ni(1)-Zr(1)/HZ catalyst increased due to the more uniform dispersion of Ni-Zr metal on the HZSM-5 surface, which prevented considerable pore blockage. The Ni(1)-Zr(2)/HZ and Ni(2)-Zr(1)/HZ catalysts have lower surface areas of 269.266 and 246.558 m²/g. The decrease in surface area is generally attributed to Ni-Zr metal species covering the HZSM-5 surface and partially blocking the zeolite channels; these results are consistent with the study by Anekwe *et al.* [31], found that the Ni-Zr species were successfully dispersed on the surface and incorporated into the pores of HZSM-5. The average pore size and pore volume of the synthesized HZSM-5 zeolite were found to be not significantly different from those of the commercial sample, as shown in Table 3. The pore sizes of the commercial and synthesized HZSM-5 were 2.559 and 2.838 nm, respectively, indicating mesopore sizes with pore volumes of 0.2213 and 0.2237 cm³/g. Anekwe *et al.* [31] found that the synthesized HZSM-5 zeolite had an average pore size of 2.224 nm, which falls within the mesopore range (2–50 nm) and a pore volume of 0.678 cm³/g. The pore sizes of the HZSM-5-based catalysts ranged from 2.559 to 3.817 nm, which fall within the mesoporous range (2–50 nm) according to the IUPAC classification. Regarding the molecular dimensions of triglycerides, Uemura *et al.* [44] reported a hydrodynamic radius of approximately 0.7–0.8 nm for individual oil molecules, corresponding to an estimated molecular diameter of 1.4–1.6 nm. Similarly, Bleaching and Purifying Fats and Oils: Theory and Practice, 2nd Edition, reports triglyceride molecular dimensions of approximately 1.5–2.0 nm [45]. These dimensions suggest that triglyceride molecules access some of the mesoporous regions of the catalysts, particularly those with larger pore diameters. However, their diffusion into the internal pores may still be restricted by pore dimensions, molecular configuration, and steric hindrance. Therefore, the transesterification reaction is expected to occur predominantly on the external catalyst surface and potentially within accessible mesoporous regions. This suggests that the catalytic performance is governed not only by the BET surface area but also by pore accessibility and the availability of active sites accessible to the triglyceride molecules.

Figure 9 depicts the pore size distribution graph of the Ni-Zr/HZ catalyst, with the highest peak occurring at 2-30 nm, corresponding to the mesopore size distribution. The average pore diameters for Ni-Zr/HZ were calculated using the BJH (Barrett-Joyner-Halenda) method and are shown in Table 3. The Ni(1)-Zr(1)/HZ, Ni(1)-

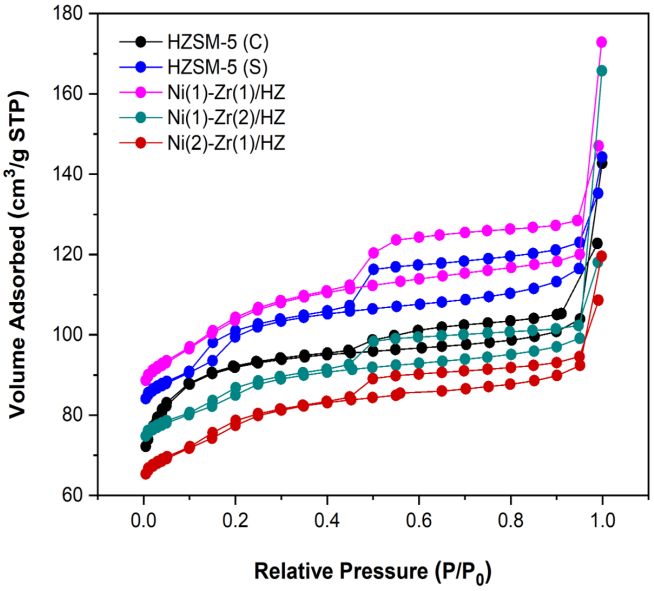


Figure 8. Langmuir Isotherm of HZSM-5 (C), HZSM-5 (S), Ni(1)-Zr(1)/HZ, Ni(1)-Zr(2)/HZ, dan Ni(2)-Zr(1)/HZ.

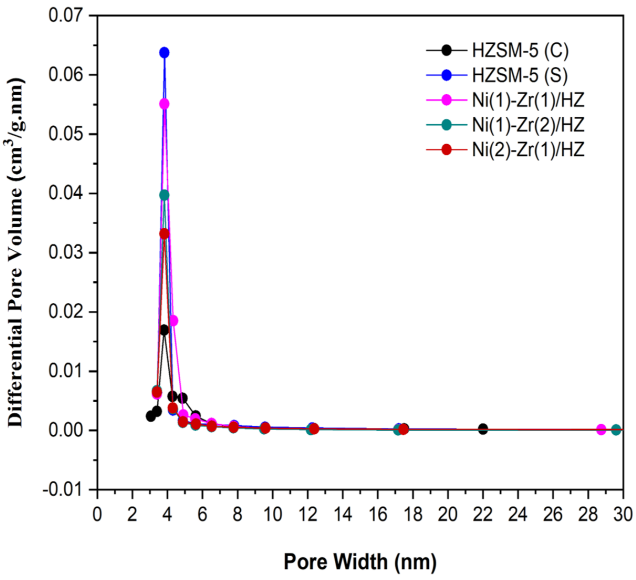


Figure 9. Pore Size Distribution of HZSM-5 (C), HZSM-5 (S), Ni(1)-Zr(1)/HZ, Ni(1)-Zr(2)/HZ, dan Ni(2)-Zr(1)/HZ.

Copyright © 2027, ISSN 1978-2993

Zr(2)/HZ, and Ni(2)-Zr(1)/HZ are 3.273, 3.817, and 3.007 nm, corresponding to mesopore diameters. The average pore size rose following metal impregnation, which is consistent with a research by Zhang *et al.* [46], found that bigger pore sizes had the ability to speed mass transfer while decreasing internal diffusion.

The Ni(2)-Zr(1)/HZ catalyst's pore volume reduced from 0.2237 cm^3/g to 0.1854 cm^3/g, which Anekwe *et al.* [31] attributed to metal species deposition that blocked the catalyst's internal channels. These findings are reinforced by studies undertaken by Al-Muttaqii *et al.* [47], found that the pore volume of oxide-phase catalysts reduces when compared to the support. This observation is consistent with the fact that metal-loaded catalysts have a lower overall pore volume than catalysts that were not impregnated with metal. Compared to the Ni(1)-Zr(1)/HZ and Ni(1)-Zr(2)/HZ catalysts, which increased pore volume to 0.2680 and 0.2570 cm^3/g, respectively. According to Niu *et al.* [40], this happens because the pore volume rises as the catalyst goes from micropores to mesopores, removing diffusion barriers and influencing product diffusion within the mesopores, resulting in improved selectivity.

The NH_3-TPD characterisation results in Figure 10 reveal that commercial and produced HZSM-5 have different acid site distributions and strengths. The HZSM-5 zeolite (C) has two major desorption regions at around 270-320 °C, indicating the existence of weak and moderate acid sites. There is also a second peak in the 600-700 °C range, which is less intense. Desorption at this high temperatures suggests the presence of strong acid sites in HZSM-5 (C). These findings indicate that commercial HZSM-5 has a highly diverse distribution of acid sites, with moderate acid sites being the most prevalent and some strong acid sites. Meanwhile, HZSM-5 (S) showed a larger desorption profile in the 220-400 °C range with lower intensity than HZSM-5 (C). These findings are also consistent with the overall acidity values provided in Table 5, which are 0.4329 mmol/g for HZSM-5 (C) and 0.4021 mmol/g for HZSM-5 (S), showing that HZSM-5 (C) contains a somewhat greater number of acid sites. These findings are similarly supported by Jia *et al.* [48], found that the nano-ZSM-5 catalyst has a total acidity of 0.4223 mmol/g at 371 °C. This study's total acidity was higher than that reported by Herlina *et al.* [49], which was only 0.361 mmol/g at around 215-271 °C for weak and moderate acids and 696 °C for strong acids. Furthermore, Che *et al.* [50] corroborate that the total acidity in this investigation is higher; ZSM-5 at 181-233 °C for weak acids and 379 °C for strong acids has a total acidity of only 0.2876 mmol/g.

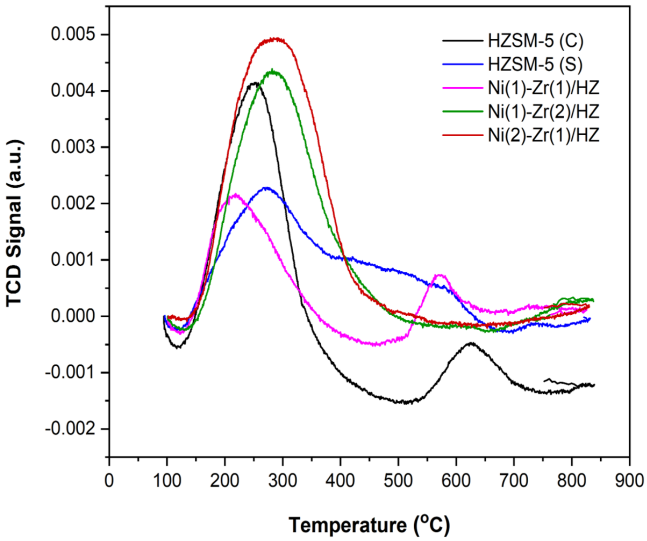


Figure 10. NH_3-TPD curved of HZSM-5 (C), HZSM-5 (S), Ni(1)-Zr(1)/HZ, Ni(1)-Zr(2)/HZ, dan Ni(2)-Zr(1)/HZ.

Modifying HZSM-5 with Ni-Zr impregnation significantly altered the NH_3-TPD profile. The Ni(1)-Zr(1)/HZ catalyst showed a low-intensity desorption peak at temperatures about 210-230 °C, confirming the presence of weak acid sites. Furthermore, a second peak at 570–620 °C reveals the existence of strong acid sites, with a total acidity of 0.2866 mmol/g. Although the total acidity is the lowest, the combination of weak and strong acid sites results in a more diverse acidity profile for the activation of carbonyl groups in triglycerides and interactions with methanol. According to Che *et al.* [50], changes in catalyst acidity result from cation exchange between metal species and protonic acids present on the catalyst surface, which turns strong acids into weak or moderate acids.

An increase in the Zr ratio in Ni(1)-Zr(2)/HZ resulted in an increase in desorption intensity at 280-330 °C, indicating a greater contribution from medium-strength acid sites with a maximum total acidity of 0.5113 mmol/g. Meanwhile, Ni(2)-Zr(1)/HZ had the maximum desorption intensity, with a major peak ranging from 270 to 350 °C and a total acidity of 0.4287 mmol/g. This profile shows that the Ni-Zr ratio of

Table 5. Acidity profile of HZSM-5 and Ni-Zr/HZ catalyst.

Catalyst	Peak Position (°C)		Acidity (mmol/g)
	Weak	Strong	
HZSM-5 (C)	270-320	600-700	0.4329
HZSM-5 (S)	220-400	-	0.4021
Ni(1)-Zr(1)/HZ	210-230	570-620	0.2866
Ni(1)-Zr(2)/HZ	280-330	-	0.5113
Ni(2)-Zr(1)/HZ	270-350	-	0.4287

Copyright © 2027, ISSN 1978-2993

2:1 produces more acid sites and a wider range of acid site strengths than other catalysts. Acidity changes are caused by Ni and Zr species interacting with HZSM-5 surface and active sites. The metals Ni and Zr can help to generate new Lewis acid sites, whereas metal interactions with the zeolite surface can alter the chemical environment of existing acid sites in HZSM-5. This is congruent with the findings of Herlina *et al*. [49], found that impregnating ZSM-5 with CuO and NiO increased the acidity from 0.361 mmol/g to 0.586 and 0.379 mmol/g for the CuO/ZSM-5 and NiO/ZSM-5 catalysts, respectively.

3.3. Effect Metal-to-Catalyst Ratio and Time Reaction

During this study, the catalytic performance of the HZSM-5 and Ni-Zr/HZ catalysts was assessed. Figure 14??? (should be numbered consecuatively) illustrates the impact of the metal-to-catalyst ratio and the transesterification reaction time. This study's yield data were examined using a multilevel factorial design (5×2) with two factors: five levels for the catalyst (HZSM-5 (C), HZSM-5 (S), Ni(1)-Zr(1)/HZ, Ni(1)-Zr(2)/HZ, and Ni(2)-Zr(1)/HZ) and two levels for transesterification reaction time (3 and 5 hours). Equation (2) represents the mathematical model based on a multilayer factorial design.

$$Y = 76.014 - 8.069X_1 - 4.129X_2 + 1.931X_3 + 1.481X_4 + 8.786X_5 - 1.206X_6 + 1.206X_7 \quad (2)$$

Figure 11 is Pareto Chart of Standardized Effects shows that catalyst (A) and reaction time (B) have a substantial effect on yield, with standardized effect values over the significance threshold of 2.776 (α = 0.05). The catalyst factor has the greatest influence, with a standardized effect value of roughly 9.2, whereas reaction time has a value of around 3.2; hence, the catalyst contributes more to variations in yield than reaction time. Furthermore, the residual diagnostic test findings in Figure 12 reveal that the dots on the Normal Probability plot tend to follow a straight line, indicating that the residuals are close to normal distribution. The residuals in the Residuals Versus Fits plot are randomly distributed about the zero line, with no discernible pattern; similarly, the Residuals Versus Order plot shows no systematic trend or pattern in terms of observation order. The

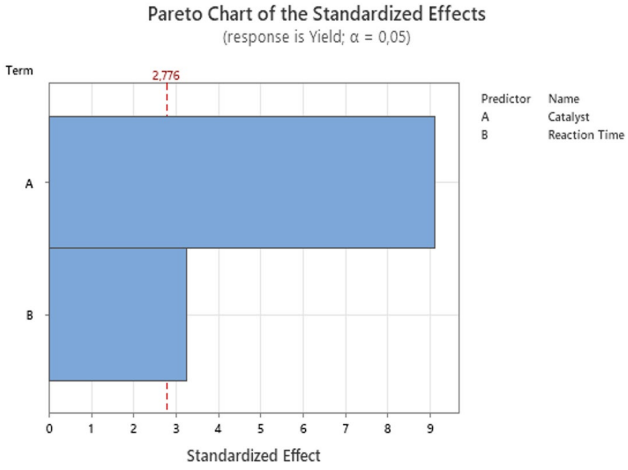


Figure 11. Statistical significance of each factor.

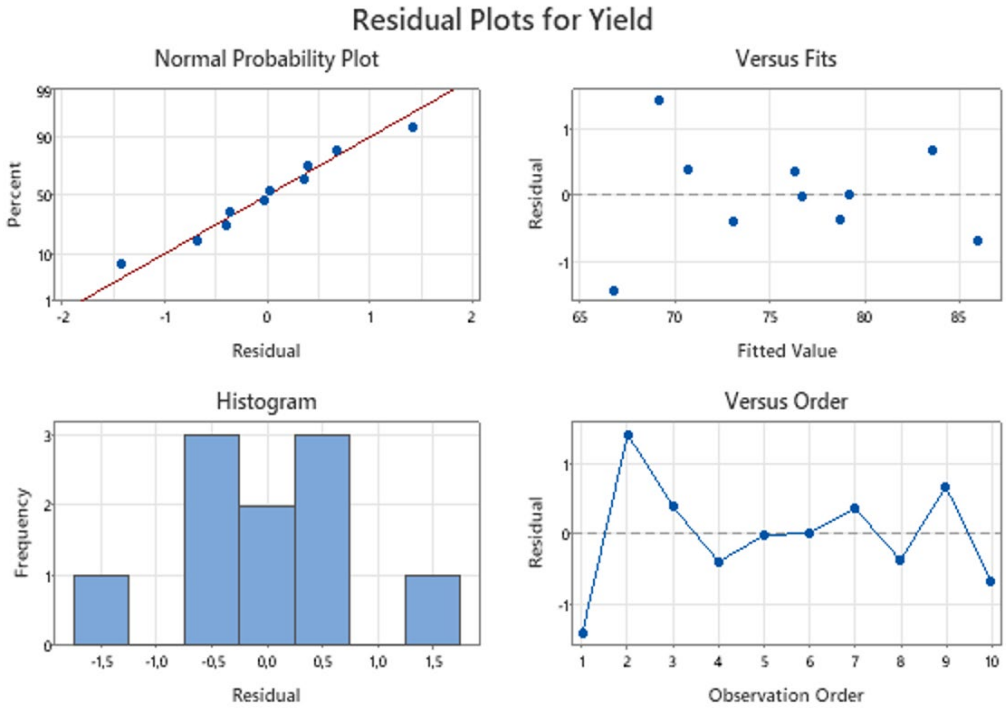


Figure 12. Diagnostic curves of the multilevel factorial design analysis.

Copyright © 2027, ISSN 1978-2993

residual histogram shows a bell-shaped pattern with a generally symmetrical distribution of data around zero, supporting the hypothesis that the residuals are approximately normally distributed. These findings are congruent with the Normal Probability plot, which indicates that the residual points generally follow a straight line. Overall, both factors have a considerable effect on yield, and the residual pattern shows that the model is well-fitted and does not violate any of the residual assumptions.

The main effects plot demonstrates in Figure 13 that the kind of catalyst has a greater impact on yield than reaction time. The average yield rose from 67.95% for HZSM (C) to a high of 84.8% for Ni(2)-Zr(1)/HZ, demonstrating that Ni-Zr impregnation improves catalytic activity significantly. Meanwhile, extending the reaction period from 3 to 5 hours increased the average yield from 74.81% to 77.22%, demonstrating that a longer reaction time allows more reactants to be transformed into biodiesel. These findings are verified by the Interaction Plot in Figure 13, which reveals that all of the lines representing the various catalyst types are virtually parallel, showing no significant interaction between catalyst type and reaction time. Overall, this trend is consistent with the Pareto Chart results, which reveal that the catalyst is the most important factor, with reaction time having a minor but still considerable effect on yield.

These findings were validated by a two-way analysis of variance (ANOVA), as shown in Table 6, which shows that the type of catalyst and reaction time have a significant effect on yield at the 95% confidence level. According to Table 6, the F-value for the catalyst factor was 59.85 with a p-value of 0.001, while the F-value for the reaction time factor was 10.53 with a p-value of 0.032. Both factors have p-values < 0.05, hence H_0 is rejected while H_1 is accepted statistically. This result is confirmed further by a comparison of the F-value to the F-crit, both the computed F-values for the catalyst and reaction duration exceed F-crit. Therefore, H_0 is rejected; there is sufficient statistical evidence to suggest that variations in catalyst type and transesterification reaction time cause significant variances in yield. Table 6 shows the findings of the two-way ANOVA on biodiesel yield.

In this investigation, Figure 14 is the effect of the catalyst on yield. Nunez *et al.* [51] found that impregnating ZSM-5 (Si/Al ratio = 50) with 5% Co improved FAME selectivity from 1.9% to 49.4%. As shown in this work, using a 5% Ni-Zr metal impregnation at ratios of 1:1, 1:2, and 2:1 resulted in progressively greater yields for HZSM-5, with maximum values of 79.17%, 78.33%, and 85.33% at a reaction time of 5 hours. Muttaqii *et al.* [52] found that impregnating natural zeolite with ZnO-TiO_2 enhanced biodiesel yield from palm oil by 60.53%, which is consistent with their findings.

Next, Figure 14 depicts the influence of transesterification reaction time in this investigation, which examined two conditions: 3 and 5 hours. Marinkovic *et al.* [53] found that longer reaction times resulted in increased FAME conversion. The results demonstrate that

Table 6. Two-way ANOVA results.

Source of Variation	SS	df	MS	F	P-value	F crit
Catalyst	330.547	4	82.637	59.85	0.001	6.39
Reaction time	14.544	1	14.544	10.53	0.032	7.71
Error	5.523	4	1.381			
Total	350.614	9				

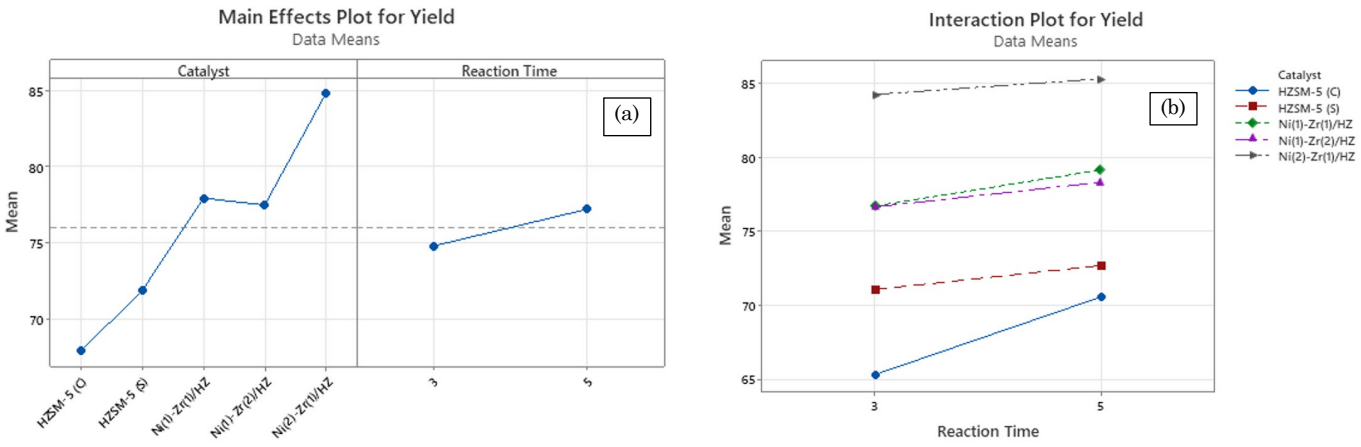


Figure 13. Main effects (a) and interaction (b) plot of experimental factor.

Copyright © 2027, ISSN 1978-2993

increasing the reaction time generally increases biodiesel yield from 65.32% at 3 h with the HZSM-5 (C) catalyst to 85.33% at 5 h with the Ni(2)-Zr(1)/HZ catalyst. With longer reaction times, triglycerides can be converted more efficiently into biodiesel, resulting in a larger yield. The comparatively minor variation in yields for the Ni(2)-Zr(1)/HZ catalyst at 3 and 5 hours (84.27% and 85.33%, respectively) suggests that the reaction was essentially complete within 3 hours. Zahra *et al.* [54] found that using the K/Al_2O_3 catalyst resulted in an increase in FAME yield over 3 and 5 hours, from 97.12% to 97.58%. The results in this study are lower because the study by Zahra *et al.* [54] used a strong base catalyst, which theoretically produces higher conversion and FAME yields. However, the K/Al_2O_3 catalyst used here is highly effective at achieving high conversion rates in a very short time approximately 1-3 hours.

4. Conclusions

Microwave-assisted bimetallic Ni-Zr impregnation successfully modified the physicochemical properties of bottom-up synthesized HZSM-5, demonstrating its effectiveness as a catalyst for the transesterification of sunflower seed oil. Characterization results obtained from XRD, SEM-EDX, BET, and NH_3-TPD confirmed that Ni-Zr incorporation influenced the crystallinity, crystal size, morphology, particle size, elemental composition, textural properties, and acidity of the zeolite. These changes demonstrate that the Ni-Zr loading ratio plays an important role in determining the physicochemical characteristics of the modified HZSM-5. Among the investigated catalysts, Ni(2)-Zr(1)/HZ exhibited the best catalytic performance, achieving biodiesel yields of 85.33% at reaction times of 5 h. The increase in yield with prolonged reaction time indicates that extending the reaction duration from 3 to 5 h enhanced biodiesel production. Overall, this study demonstrates that microwave-assisted Ni-Zr impregnation is an effective approach to modifying bottom-up synthesized HZSM-5 and improving its catalytic performance in sunflower seed oil transesterification.

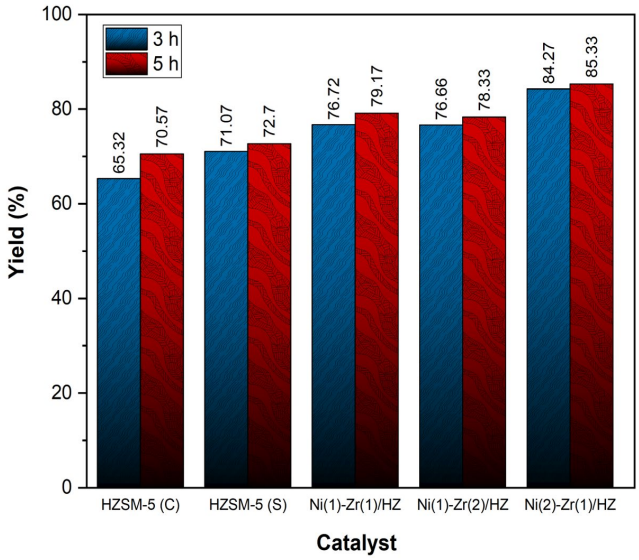


Figure 14. The effect of metal-to-catalyst rasio and transesterification reaction time on biodiesel yield.

Acknowledgements

The authors would like to express their sincere gratitude to the Process Development Research Group - Technology Innovation & Implementation (TI&I) of PT Pertamina their support, facilities, and valuable contributions to this research.

CRediT Author Statement

Authors Contributions: Muhamad Ilyas Zainul Furqon: Data analysis, Investigation, Visualization, Writing – original draft. Vernanda Febrianti: Formal analysis, Data curation. Anatta Wahyu Budiman: Writing – review & editing, Validation, Supervision, Funding acquisition, Conceptualization. Adrian Nur: Writing – review & editing, Validation. Bregas Siswahjono Tatag Sembodo: Writing – review & editing, Validation. All authors have read and agreed to the published version of the manuscript.

Declaration of Conflict of Interest

The authors declare that there are no known finansial, personal, or professional conflicts of interest that could have influenced the research, analysis, interpretation of the results, or preparation manuscript. This research was conducted independently, without any commercial or finansial relationships that could be perceived as a potential conflict of interest. Furthermore, the authors confirm that there are no competing interests, either directly or indirectly, associated with the materials, methods, results, or conclusions presented in this study. All authors have reviewed and approved the final version of the manuscript and agree with its submission for publication.

Declaration of Generative AI Use

During the preparation of this manuscript, the authors used ChatGPT (OpenAI) to assist with language editing, grammar checking, and the generation of conceptual scientific illustrations were reviewed, verified, and edited by the authors to ensure scientific accuracy. The authors take full responsibility for the content and integrity of the published work.

Copyright © 2027, ISSN 1978-2993

References

[1] Roth, W. J., Gil, B., Tarach, K., Gora-Marek, K. (2025). Top-down engineering of zeolite porosity. *Chemical Society Reviews*, *54*(16), 7484–7560. DOI: 10.1039/d5cs00319a

[2] Jia, X., Jo, C., Yip, A.C.K. (2021). Synthesis Strategies for Hierarchical Zeolites. Wiley_VCH GmbH, 119–145. DOI: 10.1002/9783527813599.ch7

[3] Aloise, A., Marino, A., Dalena, F., Giorgianni, G., Migliori, M., Frusteri, L., Cannilla, C., Bonura, G., Frusteri, F., Giordano, G. (2020). Desilicated ZSM-5 zeolite: Catalytic performances assessment in methanol to DME dehydration. *Microporous and Mesoporous Materials*, *302*, 110198. DOI: 10.1016/j.micromeso.2020.110198

[4] Sun, X., Yang, Y., He, Y., Zhu, S., Liu, Z. (2021). Stability of Zeolite HZSM-5 in Liquid Phase Dehydration of Methanol to Dimethyl Ether. *Catalysis Letters*, *151*(7), 2004–2010. DOI: 10.1007/s10562-020-03454-y

[5] Wang, J., Ma, J., Ling, L., Zhang, Y., Zhang, R., Shen, X., Li, X., Wang, B. (2024). The active site for dehydrogenation and cyclization on Zn^{2+}/HZSM-5 catalyst aiming at long-chain C6 mono-olefins aromatization. *Fuel*, *366*(79), 131362. DOI: 10.1016/j.fuel.2024.131362

[6] Pantupho, W., Neramittagapong, A., Osakoo, N., Wittayakun, J., Loiha, S. (2017). The effects of preparation methods on iron structures of iron-supported hzsm-5 and their catalytic performance for methanol dehydration. *Key Engineering Materials*, *723 KEM*, 633–639. DOI: 10.4028/www.scientific.net/KEM.723.633

[7] Kim, S., Kim, Y. T., Zhang, C., Kwak, G., Jun, K. W. (2017). Effect of Reaction Conditions on the Catalytic Dehydration of Methanol to Dimethyl Ether Over a K-modified HZSM-5 Catalyst. *Catalysis Letters*, *147*(3), 792–801. DOI: 10.1007/s10562-017-1981-0

[8] Kristiani, A., Sudiyarmanto, S., Aulia, F., Hidayati, L.N., Abimanyu, H. (2017). Metal supported on natural zeolite as catalysts for conversion of ethanol to gasoline. *MATEC Web of Conferences*, *101*. DOI: 10.1051/matecconf/201710101001

[9] Din, I.U., Alotaibi, M.A., Alharthi, A.I. (2020). Green synthesis of methanol over zeolite based Cu nano-catalysts, effect of Mg promoter. *Sustainable Chemistry and Pharmacy*, *16*(May), 100264. DOI: 10.1016/j.scp.2020.100264

[10] Frusteri, L., Bonura, G., Cannilla, C., Todaro, S., Giordano, G., Migliori, M., Frusteri, F. (2020). Promoting direct CO_2 conversion to DME over zeolite-based hybrid catalysts. *Petroleum Chemistry*, *60*, 508–515. DOI: 10.1134/S0965544120040076

[11] Liu, Yong, Lu, H. (2020). Synthesis of ZSM-5 zeolite from fly ash and its adsorption of phenol, quinoline and indole in aqueous solution. *Materials Research Express*, *7*(5). DOI: 10.1088/2053-1591/ab8fec

[12] Aviantara, D.B., Suciati, F., Hadiko, G., Indrasti, N.S., Yani, M. (2024). Microwave-assisted Impregnation of Zinc Metal Ions on Surface of Quenched Pulverized Shrimp Shell Waste. *International Journal of Technology*, *15*(6), 1946–1958. DOI: 10.14716/ijtech.v15i6.6170

[13] Jing, J., Li, L., Chu, W., Wei, Y., Jiang, C. (2018). Microwave-assisted synthesis of high performance copper-based catalysts for hydrogen production from methanol decomposition. *International Journal of Hydrogen Energy*, *43*(27), 12059–12068. DOI: 10.1016/j.ijhydene.2018.04.104

[14] Guo, X., Yin, J., Xia, S., Gong, J., He, J., Tang, F., Zuo, C., Liu, P. (2024). A novel bifunctional catalyst obtained by in situ introduction of hierarchically structured HZSM-5 for direct DME synthesis from CO_2 hydrogenation. *Fuel*, *364*, 131057. DOI: 10.1016/j.fuel.2024.131057

[15] Ren, S., Fan, X., Shang, Z., Shoemaker, W.R., Ma, L., Wu, T., Li, S., Klingho, N.B., Yu, M., Liang, X. (2020). Enhanced catalytic performance of Zr modified $CuO/ZnO/Al_2O_3$ catalyst for methanol and DME synthesis via CO_2 hydrogenation. *Journal of CO_2 Utilization*, *36*, 82–95. DOI: 10.1016/j.jcou.2019.11.013

[16] Godini, H.R., Kumar, S.R., Tadikamalla, N., Gallucci, F. (2022). Performance analysis of hybrid catalytic conversion of CO_2 to DiMethyl ether. *International Journal of Hydrogen Energy*, *47*(21), 11341–11358. DOI: 10.1016/j.ijhydene.2021.11.073

[17] Qin, L., Li, J., Zhang, S., Liu, Z., Li, S., Luo, L. (2023). Catalytic performance of Ni-Co/HZSM-5 catalysts for aromatic compound promotion in simulated bio-oil upgrading. *RSC Advances*, *13*, 7694–7702. DOI: 10.1039/d2ra07706j

[18] Liu, S., Niu, S., Yu, H., Han, K., Xia, S., Yang, Z., Zheng, Y. (2024). Electrolysis combined with magnetic CeO_2/ZSM-5@Fe_3O_4 catalyst to boost transesterification for biodiesel production. *Fuel*, *378*, 132862. DOI: 10.1016/j.fuel.2024.132862

[19] Jin, T., Fu, W., Xia, H., Zhang, Y., Zhang, L., Jia, X., Tang, T. (2024). Synthesis of transition metal-doped ETS-10 zeolite: Effect of the metal addition on the crystallization and morphology and their catalytic application for organic transformation. *Applied Catalysis A: General*, *679*(April), 119754. DOI: 10.1016/j.apcata.2024.119754

[20] Kilicaslan, M.F., Altaib, S.S., Vurdu, C.D. (2019). Effect of Ni Addition on the Morphology and Microstructure of Both Conventional Cast and Melt-Spun of Al–Si–Fe–Nb (at wt%) Alloy. *Metals and Materials International*, *25*(6), 1457–1466. DOI: 10.1007/s12540-019-00300-8

[21] Liu, Y., Gu, Y.J., Luo, G.Y., Chen, Z.L., Wu, F.Z., Dai, X.Y., Mai, Y., Li, J.Q. (2020). Ni-doped $LiFePO_4$/C as high-performance cathode composites for Li-ion batteries. *Ceramics International*, *46*(10), 14857–14863. DOI: 10.1016/j.ceramint.2020.03.011

Copyright © 2027, ISSN 1978-2993

[22] Pandiangan, K.D., Simanjuntak, W., Alista, D.I., Ilim, I. (2021). The Effect of NiO Loads on Catalytic Activity Of NiO/ZSM-5 for Transesterification of Rubber Seed Oil. *Rasayan Journal of Chemistry*, *14*(4), 2379–2385. DOI: 10.31788/RJC.2021.1446286

[23] Yusuf, B.O., Oladepo, S.A., Ganiyu, S.A. (2023). Zr-modified desilicated ZSM-5 catalysts as highly active and recyclable catalysts for production of biodiesel from soybean oil: Insight into improved catalyst properties, acidity and dispersion through desilication. *Fuel*, *351*, 128729. DOI: 10.1016/j.fuel.2023.128729

[24] Su, H., Zong, Z., Lou, W., Zhao, Q., Wang, X., Feng, X., Qi, Y., Song, Z. (2022). An Efficient Zr-ZSM-5-st Solid Acid Catalyst for the Polyol Esterification Reaction. *Catalysts*, *12*(901), 1–10. DOI: 10.3390/catal12080901

[25] Abdullah, M.H., Riyanto, O.A.W., Wulan, D.P.I. (2021). Optimization of Esterification and Transesterification Process for Biodiesel Production from Used Cooking Oil. *Journal of Research and Technology*, *7*(2), 207–216. DOI: 10.55732/jrt.v7i2.432

[26] Eldwita, K., Octhaviana, V., Rusdianasari. (2025). Production of Biodiesel from Sunflower Oil using Base Catalysts. *Asian Journal of Applied Research for Community Development and Empowerment*, *9*(1). DOI: 10.29165/ajarcde.v9i1.643

[27] Aulia, M.R., Azhari, A., Meriatna, M., Ginting, Z., Sylvia, N. (2022). Pengaruh Suhu dan Waktu Reaksi Transesterifikasi Minyak Biji Bunga Matahari terhadap Metil Ester dengan Katalis NaOH. *Chemical Engineering Journal Storage*, *2*(5). DOI: 10.29103/cejs.v2i5.8035

[28] Farouk, S.M., Tayeb, A., Abdel-Hamid, S.M.S., Osman, R.M. (2024). Recent advances in transesterification for sustainable biodiesel production , challenges , and prospects : a comprehensive review. *Environmental Science and Pollution Research*, *31*(9), 12722–12747. DOI: 10.1007/s11356-024-32027-4

[29] Guida, S., Potter, C., Jefferson, B., Soares, A. (2020). Preparation and evaluation of zeolites for ammonium removal from municipal wastewater through ion exchange process. *Scientific Reports*, *10*. DOI: 10.1038/s41598-020-69348-6

[30] Rajaei, H., Esmaeilzadeh, F., Mowla, D. (2021). Elucidation of Si / Al ratio on physicochemical properties of HZSM - 5 zeolites. *Journal of Thermal Analysis and Calorimetry*, *146*(2), 581–586. DOI: 10.1007/s10973-020-09993-1

[31] Anekwe, I.M.S., Oboirien, B., Isa, Y.M. (2024). Catalytic conversion of bioethanol over cobalt and nickel-doped HZSM-5 zeolite catalysts. *Biofuels, Bioproducts and Biorefining*, *18*(3), 686–700. DOI: 10.1002/bbb.2536

[32] Duan, H., Tian, Y., Gong, S., Zhang, B., Lu, Z., Xia, Y., Shi, Y., Qiao, C. (2020). Effect of cristallite sizes of Pt/HZSM-5 zeolite catalysts on the hydrodeoxygenation of guaiacol. *Nanomaterials*, *10*. DOI: 10.3390/nan10112246

[33] Castillo, L.A., López, O.V., García, M.A., Barbosa, S.E., Villar, M.A. (2019). Crystalline Morphology of Thermoplastic Starch/Talc Nanocomposites Induced by Thermal Processing. *Heliyon*, *5*(6). DOI: 10.1016/j.heliyon.2019.e01877

[34] Brioual, B., El-Habib, A., Rossi, Z., Aouni, A., Addou, M., Diani, M., Allah, R.F., Jbilou, M. (2025). Effect of zirconium doping on structural, optical, and electrochemical properties of NiO thin films: Electrochromic application. *Next Materials*, *6*, 100314. DOI: 10.1016/j.nxmate.2024.100314

[35] Eviva, N., Shofiyani, A., Sayekti, E. (2023). Synthesis of NaP Zeolite Based on Bauxite Red Mud Using Hydrothermal Method on Mole Ratio of SiO_2/Al_2O_3 Variations. *Positron*, *13*(1), 77. DOI: 10.26418/positron.v13i1.60099

[36] Hu, Y., Men, Y., Xu, S., Feng, Y., Wang, J., Liu, K., Zhang, Y. (2024). Modulating nickel precursors to construct highly active Ni/Y_2O_3 catalysts for CO_2 methanation. *International Journal of Hydrogen Energy*, *81*(April), 1311–1321. DOI: 10.1016/j.ijhydene.2024.07.302

[37] Chaisamphao, J., Kiatphuengporn, S., Faungnawakij, K., Donphai, W. (2021). Effect of Modified Nanoclay Surface Supported Nickel Catalyst on Carbon Dioxide Reforming of Methane. *Topics in Catalysis*, 64, 431-445. DOI: 10.1007/s11244-020-01403-y

[38] Liu, N., Chen, B., Liu, K., Qin, R., Wang, J., Zhang, Y., Zhang, Q., Gu, L., Liu, P., Cao, K., Yan, P., Fu, G., Zheng, N. . (2023). Ensemble Effect of the Nickel–Silica Interface Promotes the Water–Gas Shift Reaction. *ACS Catalysis*. 13(11), 7347-7357 DOI: 10.1021/acscatal.3c00388

[39] Adany, F., Priyanto, S., Mirzayanti, Y. W., Marbun, M.P., Furqon, M.I.Z., Kurnia, A., Hasanudin, H., Aziz, A., Edra, R., Sudibyo, S., Theo, S., Lotebulo, C., Annas, D., Yati, I., Sulaswatty, A., Nur, M., Wahyu, R., Nugroho, N., Al, M. (2025). γ-Al_2O_3-supported Cobalt and Zinc as heterogeneous catalyst for biodiesel production assisted by ultrasonic wave. *Vacuum*, *240*(May), 114502. DOI: 10.1016/j.vacuum.2025.114502

[40] Niu, P., Ren, X., Xiong, D., Ding, S., Li, Y., Wei, Z., Chen, X. (2020). Synthesis of Highly Selective and Stable Co-Cr/SAPO-34 Catalyst for the Catalytic Dehydration of Ethanol to Ethylene. *Catalysts*, *10*(7). DOI: 10.3390/catal10070785

[41] Zhang, Q., Liao, X., Liu, S., Wang, H., Zhang, Y., Zhao, Y. (2022). Tuning particle sizes and active sites of Ni/CeO_2 catalysts and their influence on maleic anhydride hydrogenation. *Nanomaterials*, 12(13), 2156. DOI: 10.3390/nano12132156

[42] Ji, K., Xun, J., Liu, P., Song, Q., Gao, J., Zhang, K. (2018). The study of methanol aromatization on transition metal modified ZSM-5 catalyst. *Chinese Journal of Chemical Engineering*, *26*(9), 1949–1953. DOI: 10.1016/j.cjche.2018.03.024

Copyright © 2027, ISSN 1978-2993

[43] Rostamizadeh, M., Yaripour, F., Hazrati, H. (2018). Ni-doped high silica HZSM-5 zeolite (Si/Al=200) nanocatalyst for the selective production of olefins from methanol. *Journal of Analytical and Applied Pyrolysis*, *132*, 1–10. DOI: 10.1016/j.jaap.2018.04.003

[44] Uemura, Y., Sinnasami, R. A., Trinh, T. H., & Onoe, K. (2020). Estimation of molecular size of triglyceride in a variety of solvents by using the intrinsic viscosity technique: An important index for transesterification of triglyceride in homogenous system. *IOP Conference Series: Earth and Environmental Science*, *460*(1). DOI: 10.1088/1755-1315/460/1/012011

[45] Patterson, H. B. W. (2009). *Bleaching and Purifying Fats and Oils: Theory and Practice 2nd Edition* (G. R. List, Ed.). AOCS Press. DOI: 10.1016/B978-1-893997-91-2.50007-9

[46] Zhang, C., Fan, K., Ma, G., Lei, C., Xu, W., J, J. (2021). Efficient synthesis of mesoporous nano ZSM-5 zeolite crystals without a mesoscale template. *Crystals*, *11*(10), 1247. DOI: 10.3390/cryst11101247

[47] Al-Muttaqii, M., Kurniawansyah, F., Prajitno, D. H., Roesyadi, A. (2019). Hydrocracking of Coconut Oil over Ni-Fe/HZSM-5 Catalyst to Produce Hydrocarbon Biofuel. *Indonesian Journal of Chemistry*, *19*(2), 319–327. DOI: 10.22146/ijc.33590.

[48] Jia, Y., Shi, Q., Wang, J., Ding, C., Zhang, K. (2020). Synthesis, characterization, and catalytic application of hierarchical nano-ZSM-5 zeolite. *Royal Society of Chemistry*, *10*, 29618–29626. DOI: 10.1039/d0ra06040b

[49] Herlina, I., Krisnandi, Y. K., Ridwan, M. (2024). Oxidation of 5-hydroxymethylfurfural into 2,5-furandicarboxylic acid over CuO dan NiO modified naturan sourced hierarchical ZSM-5. *South African Journal of Chemical Engineering*, *47*, 75–82. DOI: 10.1016/j.sajce.2023.10.011

[50] Che, Q., Yang, M., Wang, X., Yang, Q., L, W., Yang, H. (2019). Influence of physicochemical properties of metal modified ZSM-5 catalyst on benzene, toluene and xylene production from biomass catalytic pyrolysis. *Bioresource Technology*, *278*, 248–254. DOI: 10.1016/j.biortech.2019.01.081

[51] Nunez, F., Chen, L., Wang, J., Flores, S.O., Salmones, J., Arellano, U., Norena, L., Tzompantzi, F. (2022). Bifunctional Co_3O_4/ZSM-5 Mesoporous Catalysts for Biodiesel Production via Esterification of Unsaturated Omega-9 Oleic Acid. *Catalysts*, *12*(900), 1–22. DOI: 10.3390/catal12080900

[52] Muttaqii, M.A., Marbun, M.P., Priyanto, S., Sibuea, A., Simanjuntak, W., Syafaat, F., Raja, H.S., Alviany, R., Maryani, T., Sulistyaningsih, T., Prasetyo, E., Sudibyo, S., Yati, I. (2024). Muttaqii, M.A.M. *Bulletin of Chemical Reaction Engineering & Catalysis*, *19*(1), 61–68. DOI: 10.9767/bcrec.20038

[53] Marinkovic, M., Waisi, H., Blagojevic, S., Zarubica, A., Ljupkovic, R., Krstic, A., Jankovic, B. (2022). The effect of process parameters and catalyst support preparation methods on the catalytic efficiency in transesterification of sunflower oil over heterogeneous KI/Al2O3-based catalysts for biodiesel production. *Fuel*, *315*, 123246. DOI: 10.1016/J.FUEL.2022.123246

[54] Zahra, A.C., Cengko, G., Hizran, A., Rizkiana, J. (2025). Low Temperature Synthesis of Biodiesel via Heterogeneous Potassium-Alumina Catalyst. *Bulletin of Chemical Reaction Engineering & Catalysis*, *20*(2), 371–380. DOI: 10.9767/bcrec.20349

Copyright © 2027, ISSN 1978-2993